


**Interactive patches over amyloid- $\beta$  oligomers mediate fractal self-assembly**Anurag Singh , Suparna Khatun , Nisha Pawar , and Amar Nath Gupta \**Biophysics and Soft Matter Laboratory, Department of Physics, Indian Institute of Technology Kharagpur, 721302, India* (Received 23 February 2021; revised 6 November 2021; accepted 18 November 2021; published 6 December 2021)

The monomeric units of intrinsically disordered proteins self-assemble into oligomers, protofilaments, and eventually fibrils which may turn into amyloid. The aggregation of these proteins is primarily studied in bulk with no restriction on their degrees of freedom. Herein we experimentally demonstrate that amyloid- $\beta$  ( $A\beta$ ) aggregation under diffusion-limited conditions leads to its fractal self-assembly. Confocal microscopy and scanning electron microscopy with energy dispersion x-ray analysis were used to confirm that the fractal self-assemblies were formed from  $A\beta$  rather than the salt present in the two supporting media: deionized water and phosphate buffered saline. The results from the molecular docking experiments implicated that electrostatic and hydrophobic patches on the solvent-accessible surface area of the  $A\beta$  oligomers mediate the fractal self-assembly. These implications were tested with laser light scattering experiments on the oligomers formed by breaking mature fibrils of  $A\beta$  through sonication, which were observed to self-assemble into fractals when sonicated solutions were drop casted. The electrostatic interactions modulate the fractal morphologies with pH of the solution, which leads to a morphological phase transition observed through the variation in their fractal dimension. These transitions provide experimental evidence for the existing theoretical framework in terms of different kinetic models. The higher surface-to-volume ratio of these fractal self-assemblies may have applications in drug delivery, biosensing, and other biomedical applications.

DOI: [10.1103/PhysRevE.104.064404](https://doi.org/10.1103/PhysRevE.104.064404)**I. INTRODUCTION**

The complete understanding of protein aggregation under different physiological conditions is indispensable to address many unanswered questions in protein biophysics, including those related to its role in protein misfolding diseases. Notably, the misfolding of intrinsically disordered proteins (IDPs) has been linked to various neurodegenerative diseases [1]. The most studied IDP is the amyloid- $\beta$  ( $A\beta$ ) which has been investigated from different perspectives due to its physiochemical significance [2], applications in nanotechnology [3,4], and therapeutic association with Alzheimer's disease [2]. All these perspectives have  $A\beta$  aggregation at its center, where its kinetics has been intensively studied with a motive to understand its role in Alzheimer's disease and implicate the knowledge of kinetics for various applications. The possibility of an enormous number of distinct polymorphs [5] of  $A\beta$  formed during the conversion of misfolded monomers into well-defined structural units called fibrils has fascinated researchers from different scientific disciplines [6]. This is why most *in vitro* studies being conducted aim to elucidate the aggregation kinetics of proteins; hence, they are mostly performed in bulk. However, significantly less is known of the outcomes when their aggregation is monitored under diffusion-limited conditions. When a protein solution is put under diffusion-limited conditions, for instance, when drop cast on a substrate, it may lead to its fractal self-assembly. Recently, the fractal self-assemblies of different proteins have been widely observed [7–12]. However, even though different

polymorphs of  $A\beta$  are known to exist [6], there are no reports on the fractal self-assembly of  $A\beta$ .

Drop casting replicates a cellular environment where some of the degrees of freedom of proteins are restricted, leading to their biased diffusion inside the cell. As proteins have to move and interact with other biomolecules to perform their function, the biased diffusion of it may change the effects of cellular factors such as macromolecular crowding, microviscosity, and charge balance on its function. Thus, the study of protein aggregation under such conditions may decipher important aspects related to protein behavior under a degree of freedom constraint. The fractal structures of  $A\beta$  are interesting from a diagnosis and applications point of view. Even though *in vivo* observations of Alzheimer's plaques having fractal structures are not reported yet, a better understanding of oligomerization under diffusion-limited conditions might be interesting for therapeutic approaches to Alzheimer's disease. For instance, it was shown that fractal analysis of plaques can distinguish Alzheimer's disease patients from a control group [13]. Particularly, the morphological phase transition in the  $A\beta$  fractal self-assemblies as a function of pH may be beneficial for diagnosis.

The previous reports have demonstrated high sensitivity of protein self-assembly on the nature of the substrate, pH, temperature of the protein solution, and ionic strength of the media [7–12]. Also, recent studies indicate that a sufficient population of specifically sized oligomers is necessary to observe the fractal self-assembly of protein [8,9]. Herein we experimentally demonstrate that  $A\beta$  aggregation under diffusion-limited conditions leads to fractal self-assembly observed from the freshly prepared solution of  $A\beta$  in two buffer media: deionized (DI) water and phosphate buffered

\*Corresponding author: [ang@phy.iitkgp.ac.in](mailto:ang@phy.iitkgp.ac.in)

saline (PBS). The role of electrostatic interactions in modulating the fractal characteristics of the self-assembly was inspected by varying the pH of the protein solution. We further provide the experimental evidence that the observed fractal self-assemblies in DI water and PBS buffer were from the  $A\beta$  rather than the salt present in the supporting media using confocal microscopy and scanning electron microscopy (SEM) with energy dispersion x-ray (EDAX) analysis, respectively. The molecular docking experiments were performed to infer that oligomers have electrostatic and hydrophobic patches on their solvent-accessible surface area (SASA) necessary for propagating the fractal self-assembly. The matured fibrils of  $A\beta$  were broken down into smaller size aggregates (oligomers) through sonication to check the implications of the molecular docking experiments. The laser light scattering experiments on the sonicated solutions and their drop casting indicated that specific sized oligomers are necessary to mediate the fractal self-assembly.

The fractal self-assembly shows distinct morphologies governed by the repulsive electrostatic interactions, which can be modulated by changing the pH of the protein solution. Interestingly, there exist different kinetic models for fractal self-assemblies, namely, ballistic aggregation (BA) [14], diffusion-limited aggregation (DLA) [15], reaction-limited aggregation (RLA) [16], and the infinite-range mean field (MF) [17] attractive model, and the transition between these is known to exist theoretically [18–20]. However, even though the fractal morphologies resembling those expected from these models were seen experimentally [7,9], the implementation of these models, apart from DLA, to protein fractal self-assemblies is not mentioned in previous reports. Herein the fractal dimension of the morphology against changing pH of the supporting medium confirms the morphological phase transition, consistent with the transitions predicted theoretically. These results may help us understand the physicochemical interactions, which may be needed to design appropriate protein self-assemblies for desired technological applications, especially in biomedical applications [21] and construction of nanodevices [22].

## II. MATERIALS AND METHODS

### A. Sample preparation

Amyloid- $\beta$  (1-42) amino acid residue (H-DAEFRHDSGYEVHHQKLVFFAEDVGSNKGAIIGLMVGGVVIA-OH;  $M_w$ , 4515.8 g/mol) was purchased from Eurogentec, AnaSpec. A stock solution was prepared by dissolving it in pure dimethyl sulfoxide (DMSO) and sonicating it for 30 min, followed by centrifugation at 1000 rpm for 10 min to produce an aggregation-free homogeneous solution. The stock solution was diluted into two aliquots in which one contained filtered DI water [sterile and endotoxin-free 0.02  $\mu\text{m}$  polyethersulfone (PES) filter media, Whatman] and another one was filtered phosphate buffer saline (PBS buffer; 1 $\times$ , sterile and endotoxin-free 0.2  $\mu\text{m}$  PES filter media, Whatman) in such a way that the final concentration of the samples was  $\sim 10$   $\mu\text{M}$  at pH  $6.5 \pm 0.1$ , having 2% DMSO in the buffer medium. The fractal morphologies were observed at the final concentration of  $\sim 1$   $\mu\text{M}$ . All the

observations were made in an environment with 50%–60% humidity at 20  $^\circ\text{C}$ .

### B. Optical microscopy

The as-prepared  $A\beta$  solution was drop casted and allowed to dry on a cleaned coverslip under ambient conditions. An optical microscope (Nikon Eclipse Ti-U) in transmission mode with a 100 $\times$  objective lens was used to record the fractal morphologies.

### C. Confocal microscopy

Thioflavin T (ThT) fluorescent dye was added to the  $A\beta$  solution containing DI water in a molar ratio of 5:1 and incubated for 1 hr at room temperature. Then the solution was drop casted on thoroughly cleaned coverslips and left to dry before imaging for 1 hr under ambient conditions. Confocal microscopy imaging was carried out using an Olympus FlowView FV1000. The laser excitation wavelength was 405 nm.

### D. Field emission scanning electron microscopy (FESEM)

Two microliters of  $A\beta$  solution with PBS as the buffer media was drop casted on a thoroughly cleaned glass substrate and allowed to dry under ambient conditions. The gold coating was done on the surface of the dried sample to make it conductive. FESEM (Carl Zeiss SUPRA 40) was used to scan the samples at different magnification levels. Elemental mapping of the morphologies were performed using EDAX analysis to estimate the contribution of different elements in the fractal self-assembly.

### E. Dynamic/static light scattering (D/SLS)

A D/SLS (Photocor Ltd.) experiment was performed using a Ga-As diode laser operated at a wavelength of 658.3 nm, having a constant output power of 35 mW. Data analysis was done using Photocor-FC and DynaLS software. The hydrodynamic radius ( $R_H$ ) was calculated using the Stokes-Einstein relation [23],  $R_H = k_B T / 6\pi\eta D_t$ , where  $k_B$  is the Boltzmann constant,  $T$  is the temperature in Kelvin,  $\eta$  is the solvent viscosity, and  $D_t$  is the translational diffusion coefficient. In the SLS experiment, the angular dependent time-averaged scattered intensities of solvent, solution, and standard sample as a reference were recorded. For a very dilute solution, the time-averaged scattered intensity was fitted with a general equation given by,  $\frac{Kc}{R_\theta} = \frac{1}{M_w} + \frac{R_g^2 q^2}{3M_w}$ , where  $K = \frac{4\pi^2 n^2 (\frac{\partial n}{\partial c})^2}{\lambda^4 N_A}$  is the optical constant,  $n$  is the refractive index of the solvent, the position of the detector defines the scattering angle ( $\theta$ ),  $c$  is the concentration of the sample,  $\frac{\partial n}{\partial c}$  is the increment of the refractive index of the solution,  $N_A$  is Avogadro's constant,  $R_\theta$  is the Rayleigh ratio, and  $q = \frac{4\pi n}{\lambda} \sin \frac{\theta}{2}$  is the scattering vector [24]. The  $R_g$  value was estimated from the slope of the partial Zimm plot (i.e.,  $\frac{Kc}{R_\theta}$  vs  $q^2$ ).

### F. Fractal dimension calculation

The fractal dimension ( $d_f$ ) of the experimental fractal-like structures was calculated using ImageJ software [25]. The

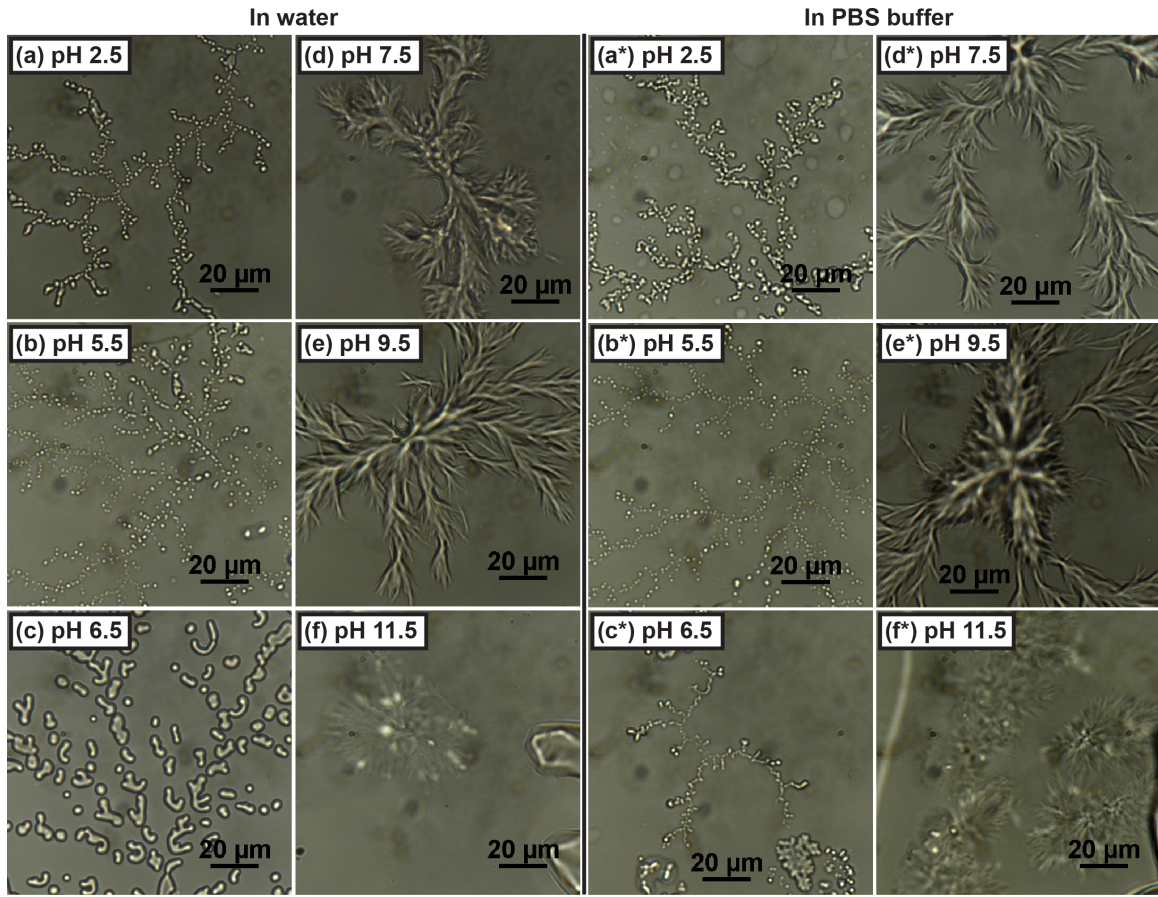


FIG. 1. The fractal morphologies were obtained from the freshly prepared solution of  $A\beta$  in (a)–(f) DI water and in (a\*)–(f\*) PBS buffer, respectively, at different pH.

images were converted to a 16-bit binary format, and  $d_f$  was calculated using the box-counting algorithm with box values of 2, 4, 8, 16, 32, 64, 128, 256, and 512 [26]. The linear regression of the line drawn between the  $\log(\text{size})$  vs  $\log(\text{count})$  determined the slope. The negative of the resultant slope represents  $d_f$  of the image.

### III. RESULTS AND DISCUSSIONS

#### A. Fractal self-assembly of $A\beta$

In the process of studying the matured fibrils of human amylin, a 37-residue peptide associated with type II diabetes mellitus [9], we recently discovered that oligomers could self-assemble into fractal-like structures under diffusion-limited conditions (drop cast on a substrate) [9]. We found that a sufficient number of specifically sized oligomers were necessary to observe fractal self-assembly of amylin, exemplifying that an intrinsically disordered protein can self-assemble into structures having fractal-like characteristics. These results motivated us to examine the  $A\beta$  peptide for fractal self-assembly. Interestingly,  $A\beta$  was also found to self-assemble into fractal morphologies under similar experimental protocols (see the experimental section) as we see for amylin, qualitatively following similar sufficient conditions required for its oligomers to self-assemble into fractals. In addition to this, other interesting features were also observed in the case of  $A\beta$ .

Figure 1 summarizes the fractal morphologies of  $A\beta$  observed in DI water and PBS buffer at different pH. In DI water, at acidic pH  $2.5 \pm 0.1$ ,  $5.5 \pm 0.1$ , and  $6.5 \pm 0.1$ , dendritic structures were observed [Figs. 1(a)–1(c)]. The branches of the fractals were thin and broken. The thickness and the feature of broken branches became more evident with the pH increase from  $2.5 \pm 0.1$  to  $6.5 \pm 0.1$ . The broken branches indicate that the DI water was acting as a mediator between the oligomers and cluster-cluster aggregation [27] as a possible mechanism behind the formation of the fractal structures. The presence of mobile water within the intersheet region [28] and its role in protein folding and assembly of  $A\beta$  fibrils [29] were recently reported. Moreover, the dehydration-driven changes in the fractal self-assembly of gelatin are already known [30]. At basic pH  $7.5 \pm 0.1$ ,  $9.5 \pm 0.1$ , and  $11.5 \pm 0.1$  [Figs. 1(d)–1(f)], in contrast, we observed dense and compact morphology. The compactness of the structures increased with an increase in the pH from  $7.5 \pm 0.1$  to  $11.5 \pm 0.1$ . With an increase in pH, the morphologies seem to become denser and cover a lesser amount of space. The  $d_f$  of the morphologies obtained at pH 7.5 to 11.5 also increased (shown later), indirectly indicating the increased compactness of the structures.

In PBS buffer, in acidic pH regimes [Figs. 1(a\*)–1(c\*)], almost similar morphologies were observed as in DI water. The difference is that the broken branches feature became less evident with an increase in the pH. At pH  $6.5 \pm 0.1$ , some oligomers were also observed near the fractal self-assembly.

At basic pH [Figs. 1(d\*)–1(f\*)], not precisely the same, but similar dense and compact structures were observed as seen in the DI water. The differences in the morphological features of the self-assemblies were attributed to the variation in the electrostatic interaction in the presence of two different media. Since the pI of  $A\beta$  used for experiments was  $\sim 6.67$ , very close to neutral pH, the charge on  $A\beta$  is close to zero. With an increase or decrease in pH from the pI of the protein, the charge on  $A\beta$  will become more negative or positive. The change in pH may alter the behavior of charged residues from hydrophilic to hydrophobic-like [31], influencing the stability of the formed oligomers. Under higher or lower pH, the oligomers may be unstable, leading to the exposure of their hydrophobic core to the solvent [32]. Therefore, the change in pH can affect both the electrostatic- and hydrophobic-driven interactions, which may play a vital role in determining the interactions between the oligomers.

### B. Evidence for the fractal self-assemblies of $A\beta$

Recently we observed that the buffer media can also self-assemble into fractals with different fractal characteristics than amylin [9]. Thus, we first confirmed that the fractal morphologies were from the  $A\beta$  and its oligomers rather than the buffer media.

#### 1. Fractal self-assembly of $A\beta$ in DI water

The confocal microscopy with the fluorescence of ThT at an excitation wavelength of 405 nm was employed for the morphologies obtained in DI water. The fluorescence of ThT has been widely used to study the aggregation kinetics, where the binding of ThT to the  $\beta$ -sheet structures of  $A\beta$  is necessary to gain the fluorescence signal [33]. The observed morphologies (Fig. 2) were not exactly similar to that observed using the optical microscope (Fig. 1), but still a transition in the morphologies from dendritic structures to dense and compact structures with an increase in pH can be seen. The differences in the morphologies shown in Fig. 1 and Fig. 2 are attributed to the presence of ThT, which may perturb the interactions responsible for the self-assembly. Similar modulations in the aggregation kinetics of  $A\beta$  were observed in the presence of ThT [34]. The nonconfocal mode images at  $\text{pH } 6.5 \pm 0.1$  [Fig. 2(c)] and  $7.5 \pm 0.1$  [Fig. 2(d)] indicate that ThT itself is capable to self-assemble into a fractal with both directional and nondirectional features, respectively. But since they were partly bound to the  $\beta$ -sheet structures of  $A\beta$  at  $\text{pH } 6.5 \pm 0.1$  and were not bound at all at  $\text{pH } 7.5 \pm 0.1$ , these self-assemblies of ThT were present in the corresponding confocal mode images with a different color (yellowish-green) [Fig. 2(c\*)] and totally absent [Fig. 2(d\*)], respectively. This indicates that ThT binding to the  $\beta$ -sheet structures of  $A\beta$  is pH-dependent. Moreover, at  $\text{pH } 6.5 \pm 0.1$ , the presence of oligomers, in both the confocal mode [Fig. 2(c)] and nonconfocal mode [Fig. 2(c\*)], images can be seen. It is important to note that the ThT-induced perturbations in the morphologies of the self-assemblies are small, and the methodology can be efficiently used to confirm the presence of proteins in the fractal self-assemblies formed in DI water.

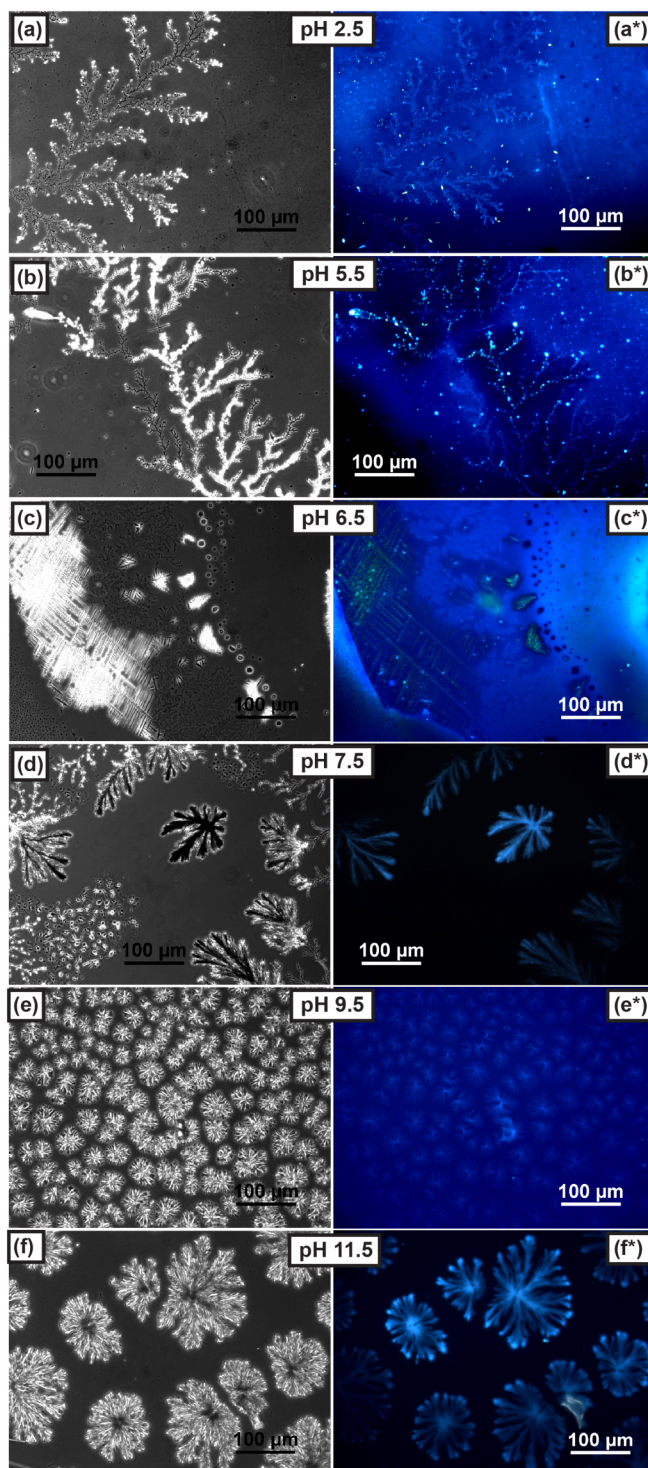


FIG. 2. The nonconfocal (a)–(f) and confocal mode (a\*)–(f\*) images of the morphologies obtained from the freshly prepared solution of  $A\beta$  in the DI water at different pH.

#### 2. Fractal self-assembly of $A\beta$ in PBS buffer

The salts present in the buffer may induce and modulate the self-assembly of proteins [30,36,37]. Therefore, for the fractal morphologies obtained in PBS buffer, the presence of  $A\beta$  was confirmed by first visualizing the fractal morphologies through SEM [Figs. 3(a)–3(f)] and then performing EDAX

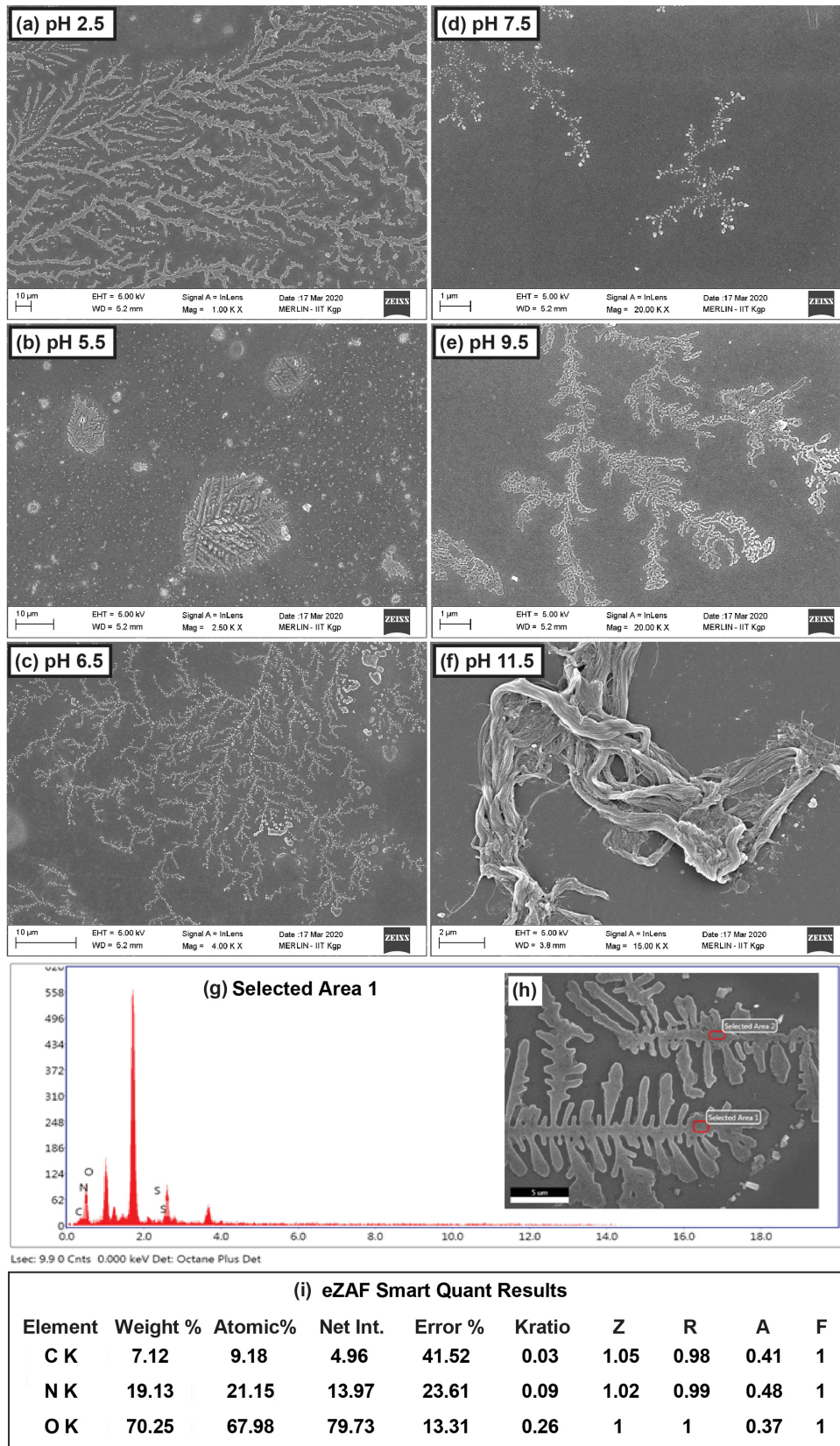


FIG. 3. The SEM images of the morphologies obtained from the freshly prepared solution of  $A\beta$  in PBS buffer at (a)–(f) different pH. (g) The energy dispersion x-ray (EDAX) spectra show the elements present in the areas chosen in the fractal morphology obtained at  $\text{pH } 6.5 \pm 0.1$ , shown in (h) for selected area 1 (see Sec. S1, Supplemental Material [35] for selected area 2). (i) The weight and atomic contributions of the elements in the EDAX spectra shown in (g).

analysis on some chosen areas on the fractal morphology [Figs. 3(g)–3(i)]. The morphologies observed through SEM were different from those observed through optical and confocal microscopy. This discrepancy may be due to the long incubation time required in SEM before imaging and a different substrate, which may modulate electrostatic contribution in the self-assembly. At pH  $2.5 \pm 0.1$  [Fig. 3(a)],  $5.5 \pm 0.1$  [Fig. 3(b)], and  $6.5 \pm 0.1$  [Fig. 3(c)] thick branched dendritic structures, compact structures with circular envelopes, and thin branched dendritic structures were observed, respectively, which were more prominent than the similar fractal morphologies observed at pH  $7.5 \pm 0.1$  [Fig. 3(d)]. At pH  $9.5 \pm 0.1$  [Fig. 3(e)], the dendritic feature was retained with thicker branches. Notably, instead of fractal structures, fibrils were observed at pH  $11.5 \pm 0.1$  [Fig. 3(f)]. The higher aggregation rate [evident from the higher values of  $R_g$ ; see Fig. 6(a) below] at pH  $11.5 \pm 0.1$  and the fact that the sample was allowed to completely dry overnight lead to the observation of fibrils at this pH. These fibrils belong to another interesting regime that is accessed when aggregation of  $A\beta$  is performed in bulk. The EDAX analysis [Fig. 3(g)], when performed on an area chosen on the structures at pH  $6.5 \pm 0.1$  [Fig. 3(h)], reveals the contribution of different elements, as shown in Fig. 3(i). Since the PBS buffer does not contain nitrogen, the significant presence of nitrogen may be used as an indicator of protein present in the self-assembly. We used this protocol to verify that the fractal morphologies were formed from protein oligomers. However, this does not guarantee the absence of salt in the PBS buffer from the observed morphologies, which may mediate the self-assembly.

### C. Role of electrostatic and hydrophobic patches

The molecular docking experiments were performed to understand the possible interactions involved in the fractal self-assembly. The electrostatic and hydrophobic interactions are two vital interactions that may lead to fractal self-assembly. The docking study provides the position and the fractional coverage of electrostatic and hydrophobic patches on the oligomers. The ClusPro webserver [39] used for molecular docking provides advantageous alternatives wherein electrostatic- and hydrophobic-based docking is feasible. We performed the docking of the modeled  $A\beta$  monomer with a  $\beta$ -sheet structure [38] [Fig. 4(a)] in a sequential (monomer-by-monomer) manner to form oligomers up to eicosamer.  $A\beta$  consists of four polar, 12 ionic, and 26 hydrophobic residues. There are three electrostatic patches [EP1(R5-S8), EP2(H13-K16), and EP3(S26-K28)] and two hydrophobic patches [HP1(L17-A21) and HP2(G29-A42)] on the SASA of the  $A\beta$  monomer [Fig. 4(b)] which were also present when the monomers were docked [Fig. 4(c)]. A nearly linear increase in the SASA of the docked structures with an increase in the oligomer size was observed [Figs. 4(d) and 4(e)]. The SASA of the docked structures, polar or ionic, and hydrophobic residues obtained from the electrostatic [Fig. 4(d)] [hydrophobic; Fig. 4(e)] represents the case where there is a nonzero (zero) charge on the protein monomers; hence, it represents the scenarios of experiments performed at pH greater or smaller than the pI (electrostatic based) and the pI (hydrophobic based), respectively. The polar or ionic or hy-

drophobic patches on the oligomers should not be exhausted for the successful evolution of the oligomers into fractal self-assemblies [Figs. 4(d\*) and 4(e\*)]. It is noted that, despite the fractional SASA decreases with the oligomer size, nonzero electrostatic and hydrophobic patches were still present [Figs. 4(d\*) and 4(e\*)] on the SASA of the oligomers. This was inspected by examining the docked structures in different orientations to ensure that there remains a polar or ionic or hydrophobic patch on the SASA of the oligomer to propagate the self-assembly further (see Sec. S2, Supplemental Material [35] for interface residues in the docked structures). A similar molecular docking study was performed with the  $A\beta$  dimer having the PDB ID-5AEF (15–42 residues) [40] (see Sec. S3, Supplemental Material [35]) to further cross-check the nonexhaustive presence of electrostatic and hydrophobic patches on the SASA of the docked structures. Notably, electrostatic and hydrophobic patches were necessary to further propagate the fractal self-assembly.

The implications of the molecular docking experiments were tested from the light scattering study conducted on the matured fibrils of  $A\beta$  formed at pH  $6.5 \pm 0.1$ . When the matured fibrils of  $A\beta$ , which themselves did not form fractal self-assembly, were sonicated (at ultrasonic power of 250 W applied for 15 s at an interval of 15 s) and drop casted, it led to an observation of fractal self-assemblies. The sonication of matured fibrils breaks them into oligomers and small protofilaments, which then diffuse on the substrate to self-assemble into fractal-like morphologies. Similar observations were made for matured fibrils of human amylin [9]. First, the presence of matured fibrils was confirmed in the  $A\beta$  solution [Fig. 5(a)]. Then the sonication was performed for 2 min, 5 min, 10 min, 15 min, and 30 min, and the corresponding size distribution of the solution was determined using DLS (Fig. 5).

With an increase in the sonication time, the extent of breakage of the fibrils was greater. This was reflected in the comparative observation of two structural features: (1) dense and compact fractal self-assembly formed over a clump of fibrils and (2) the fractal self-assembly, similar to those observed with a freshly prepared solution of  $A\beta$  at pH  $6.5 \pm 0.1$ . In the solution of matured fibrils, the structures of type (1) were scarcely present, depicted by the more significant contribution from the larger size aggregates in DLS [Fig. 5(a\*)]. However, after 2 min sonication, the population of type (1) structures increased significantly [Fig. 5(b) and see Sec. S4, Supplemental Material [35]] reflected in DLS, where the conversion of larger size aggregates into smaller aggregates can be seen [Fig. 5(b\*)]. The consistency of the result from the DLS measurement was further corroborated with TEM imaging of the broken fibrils in the solution obtained after 2 min sonication (see Sec. S4, Supplemental Material [35]). As a small span (2 min) of sonication was used, this may be due to the breakage of fibrils into structures that were bonded via weak interactions. Interestingly, with a further increase in the sonication time, the number of type (1) structures decreased, and type (2) structures increased [Figs. 5(c)–5(f)]. A similar trend in the DLS data was observed where the population of the smaller size aggregates gradually dominates over that of the larger size aggregates [Figs. 5(c\*)–5(f\*)]. This may be because a larger time of sonication leads to the breakage

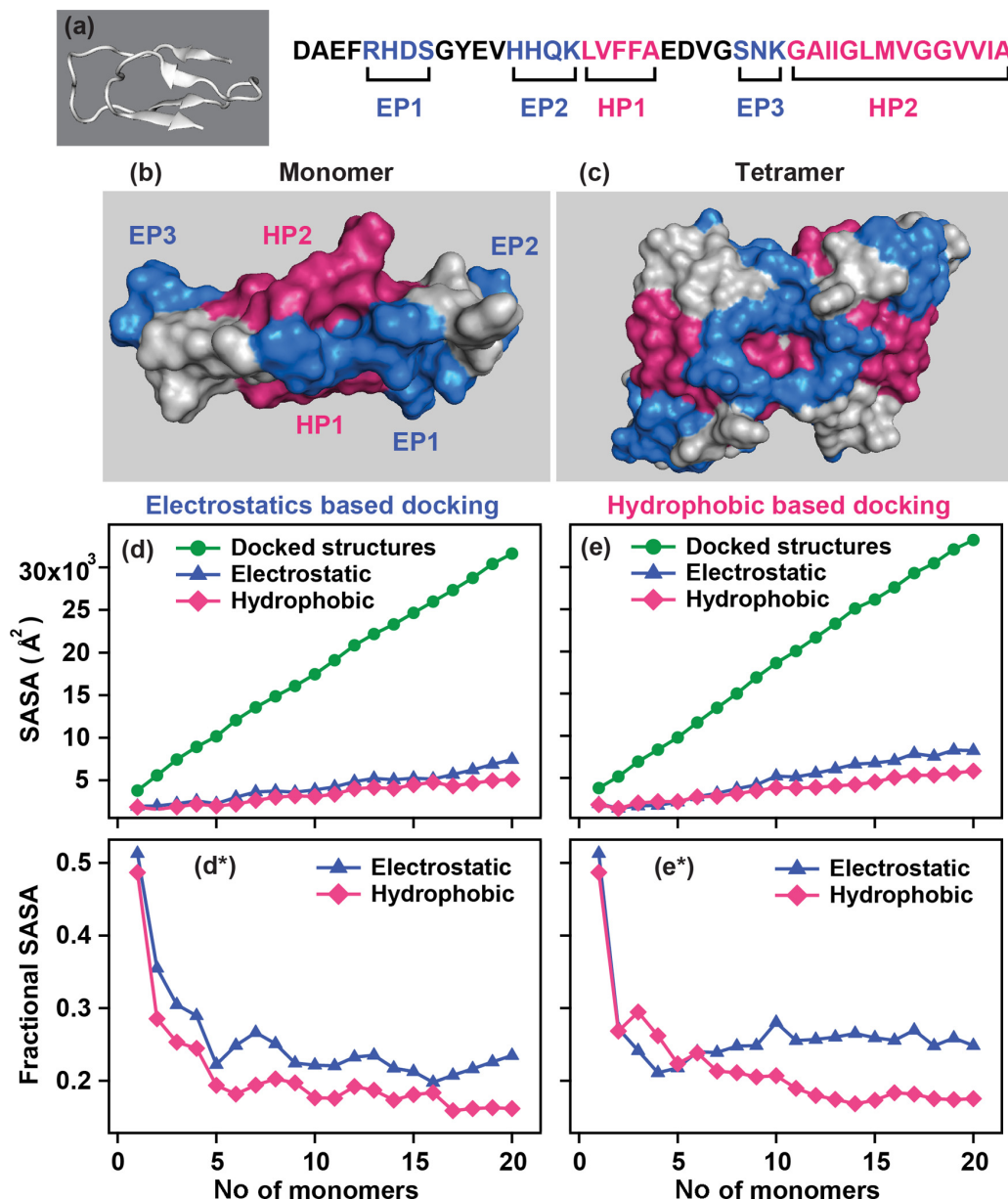


FIG. 4. The molecular docking was performed on the (a) modeled structure of A $\beta$  monomer with  $\beta$ -sheet structure [38] obtained from Dr. Bogdan Barz, Forschungszentrum Jülich, Germany. The electrostatic and hydrophobic patches on the (b) monomer and (c) docked tetramer. SASA of the docked structures and interactive patches formed using (d) electrostatics-based and (e) hydrophobic-based docking, respectively. The fractional SASA of the polar and ionic and hydrophobic residues on the SASA of the docked structures formed using (d\*) electrostatics-based and (e\*) hydrophobic-based docking, respectively.

of fibrils into smaller oligomers, hence resulting in fractal morphology similar to the self-assembly when the same size oligomers were formed from the monomeric solution of A $\beta$  [Fig. 1(c\*)].

The process through which the results of Fig. 5 were obtained can be seen as a reverse process wherein instead of being formed from the monomeric solution of A $\beta$ , the oligomers were formed by breaking fibrils through sonication and were observed to self-assemble into fractals when drop casted (Fig. 5). Surprisingly, similar morphologies observed [Fig. 1(c\*) and Figs. 5(c)–5(f)] through these reverse processes suggest that it is the oligomers that self-assemble into fractals. It is to be noted that the size (branches) of the fractal

self-assembly decreases (increases) with the increase in the sonication time. These observations indicate that specifically sized oligomers, present in a sufficient amount, are necessary for providing the fractal structural feature to the self-assembly of A $\beta$ .

In a protein solution, the hydrophobic interactions, which are fewer compared to the electrostatic interactions, may modulate the electrostatics by changing the effective charge  $q_{\text{eff}}$  on the oligomers [41–45]. The  $q_{\text{eff}}$  may also be changed by changing the pH of the protein solution [8,9,12]. The higher  $q_{\text{eff}}$  means higher repulsive interactions between the oligomers. In the presence of sufficient  $q_{\text{eff}}$ , the oligomers may be stable, and thus instead of fractal self-assembly,

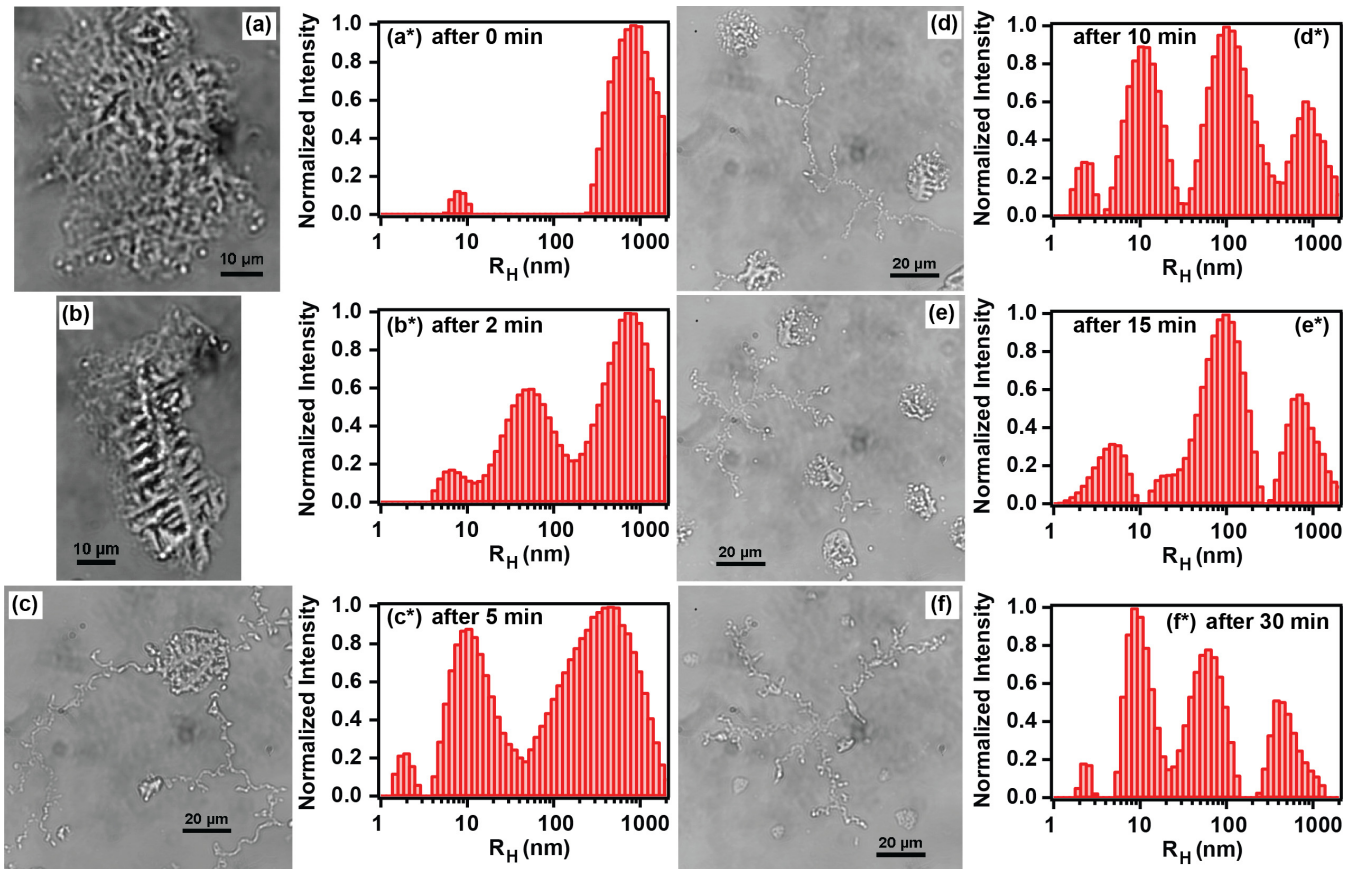


FIG. 5. The optical microscope images and the corresponding size distribution measured using DLS for matured fibrils after (a) and (a\*) 0 min, and  $A\beta$  solution of matured fibrils after sonication time of (b) and (b\*) 2 min; (c) and (c\*) 5 min; (d) and (d\*) 10 min; (e) and (e\*) 15 min; and (f) and (f\*) 30 min.

chainlike morphologies will be observed (see Sec. S5, Supplemental Material [35]). Also, the charges on the substrate may disturb the dynamics necessary for self-assembly. However, during the formation of fractal self-assembly, the uncovered hydrophobic patches on the SASA of the oligomers would try to get covered in order to decrease the free energy. So, in an energetically favored self-assembled system, the hydrophobic patches will be hidden inside the self-assembly, and the electrostatic patches will be oriented to have minimum repulsive interaction. As the effective charge in the protein solution is increased, more compact and smaller self-assemblies were evident. This indicates that when there is a large effective charge on the oligomers, the formation kinetics of the fractal self-assembly is different. However, the DLA model can explain the formation of these self-assemblies at intermediate pH, i.e.,  $5.5 \pm 0.1$  and  $6.5 \pm 0.1$ , where the effective charge on the oligomers is not large enough.

It is interesting to note an attractive feature in the fractal self-assemblies at  $\text{pH } 7.5 \pm 0.1$  to  $\text{pH } 11.5 \pm 0.1$  (Fig. 1 and Fig. 2). At  $\text{pH } 7.5 \pm 0.1$  and  $9.5 \pm 0.1$ , there is an indication that the central point of the fractal act as a bifurcation point for the morphology. The bifurcation characteristics became even more apparent at  $\text{pH } 11.5 \pm 0.1$ . This indicates the presence of other parameters, the interplay between which affects the shape plasticity of the self-assembly [46]. The previous results also suggest that the surface thermodynamics and the crystal morphologies are related [47]. The

detailed study of the presence of a bifurcation point in these fractal self-assemblies is the subject matter of our ongoing investigation.

#### D. Morphological phase transition in the fractal self-assembly of $A\beta$

A careful inspection of the morphologies, in both DI water and PBS buffer (Fig. 1), indicated the presence of a morphological phase transition in the fractal self-assembly of  $A\beta$ . Theoretically, the growth probability  $P$  of the fractal morphologies can be described by the spatial variation of a potential field  $\Omega$ ,  $P \propto |\nabla\Omega|^\alpha$ , with scaling parameter  $\alpha$ . The transition in the morphologies can be realized by varying  $\alpha$  [48,49]. Different  $\alpha$  depicts the level of screening and anisotropy in the system, which in turn decides different regimes of fractal growth.  $\alpha = 0$  depicts BA where the particles move in a straight line giving rise to compact and dense fractals;  $\alpha = 1$  represents the ideal Laplacian growth of which DLA is a well-known example and RLA when repulsive electrostatic interactions are involved; and when  $\alpha \rightarrow \infty$ , the long-range interactions dominate over the stochasticity of the process and can be described by MF attractive model. The transitions between the morphologies obtained using these models have been shown to exist theoretically.

Interestingly, the morphological transitions in the fractal self-assembly of  $A\beta$  observed herein provide experimental



TABLE I. The fractal growth regime; RLA-DLA and DLA-BA transitions in the obtained fractal morphologies of  $A\beta$ .

pH	Fractal self-assembly in DI water	Fractal self-assembly in PBS buffer
$2.5 \pm 0.1$	RLA	RLA
$5.5 \pm 0.1$	RLA	RLA-DLA
$6.5 \pm 0.1$	RLA-DLA	DLA
$7.5 \pm 0.1$	BA	DLA-BA
$9.5 \pm 0.1$	BA	BA
$11.5 \pm 0.1$	BA	BA

evidence for such transitions summarized in Table I. The assignment of the kinetic growth regime to the observed fractal morphologies was done by checking their similarity with those expected through the application of the models [19]. The emergence of DLA-BA transition in PBS buffer and its absence in DI water indicate that the  $A\beta$  solution is more stable in PBS buffer than in DI water.

The realizations of these transitions can be obtained by estimating the evolution of  $R_g$  of the protein aggregates with time at similar pH for which the fractal morphologies were obtained [Fig. 6(a)], and the  $d_f$  of fractal structures observed in both DI water and PBS buffer [Fig. 6(b)], which provides a signature for these transitions. Figure 6(a) indicates that  $A\beta$  aggregation is highly pH-dependent, consistent with the previous reports [50]. At  $\text{pH } 11.5 \pm 0.1$ , the oligomer formation would be faster, and since the size of the oligomer will be greater (and hence less stochastic), it leads to an effective straight-line motion of the oligomers, resulting in BA. The decrement in the fluctuations with size has been recently reported for gold nanoparticles [51]. The BA is also an outcome of screening long-range hydrophobic interactions [52] due to nonzero charge on the oligomers. The electrostatic and hydrophobic patches on the surface of oligomers, formed under diffusion-limited conditions, decide the complexity of the fractal self-assembly of  $A\beta$  [Fig. 6(b)]. Near the pI ( $= 6.67$ ), the electrostatic interactions are minimum, and long-range hydrophobic attractive interactions govern fractal formation. Hence, in a very small pH regime, close to pI, fractal formation is described by MF where chainlike morphologies are expected. Even though we observed chainlike morphologies at  $\text{pH } 6.5 \pm 0.1$  (see Sec. S5, Supplemental Material [35]), it is very difficult to pinpoint the pH regime in which MF will dominate over DLA. In the acidic regime, as supported by  $R_g$ , neither the oligomers' size is large enough to eradicate the effect of stochasticity, nor are the hydrophobic interactions effectively screened, leading to large stochasticity, hence resulting in RLA governed structures. So, at  $\text{pH } 2.5 \pm 0.1$ ,  $6.5 \pm 0.1$ , and  $11.5 \pm 0.1$ , RLA-, DLA-, and BA-based structures were observed, respectively. Furthermore, between pH values, the morphologies are in the state of transitions between these kinetic models, evident from the mixed morphological features.

The dendritic DLA-like structures were observed at  $\text{pH } 6.5 \pm 0.1$ . The observations at  $\text{pH } 2.5 \pm 0.1$  and  $5.5 \pm 0.1$  suggest that there is a positive charge on the oligomers

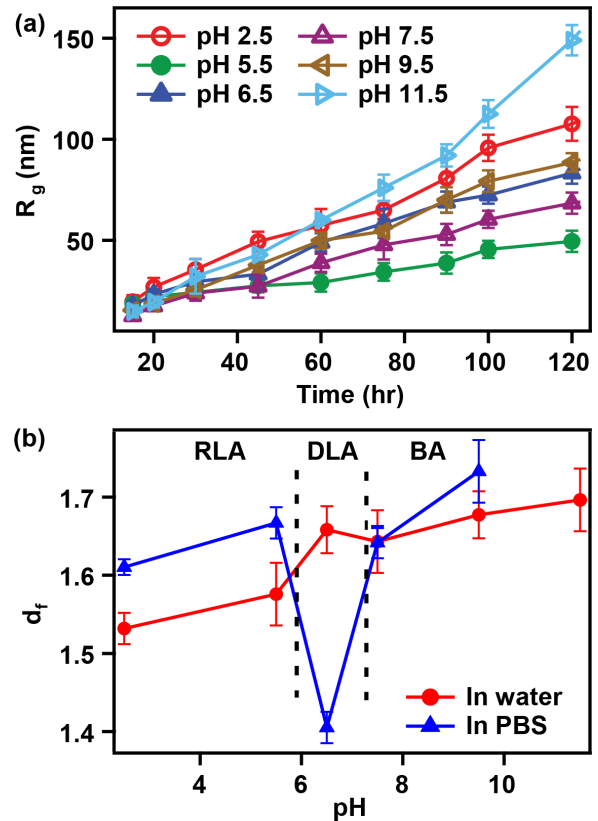


FIG. 6. (a) The radius of gyration ( $R_g$ ) of  $A\beta$  aggregation as a function of time measured for 5 days at similar pH for which the fractal morphologies were observed. (b) The  $d_f$  as a function of pH; it depicts a morphological phase transition in the fractal self-assembly of  $A\beta$ . The  $d_f$  for fractal self-assembly obtained in PBS buffer at  $\text{pH } 11.5 \pm 0.1$  is not shown due to inaccuracy in the  $d_f$  mainly because of the contrast of the image (see Sec. S6, Supplemental Material [35]).

indicating RLA as possible kinetics responsible for the morphology observed experimentally. At  $\text{pH } 7.5 \pm 0.1$ ,  $9.5 \pm 0.1$ , and  $11.5 \pm 0.1$ , not only is there a net negative charge on the oligomers, but there is also a high probability for these oligomers to self-assemble into protofilaments which may be responsible for providing dense nondendritic structures. This again indicates that, at these pH, other aggregation kinetics (BA) is necessary to explain its formation.

The transitions RLA-DLA and DLA-BA between the kinetic models can be better understood in terms of a mixing parameter  $m$  [19], which decides which of the two, stochastic or energetics, dominates the growth process. Theoretically, it is predicted that the stochasticity dominates for  $m < 0.01$  and energetics dominates when  $m \rightarrow 1$ . However, the transitions RLA-DLA and DLA-BA were observed at  $m = 0.1$  itself [19]. In the case of  $A\beta$ , the mixing parameter  $m$  depicts the contribution of electrostatic and hydrophobic interactions in the self-assemblies. From the observed morphological transitions [Fig. 1 and Fig. 6(b)], it is evident that the interactions dominate at  $\text{pH } 2.5 \pm 0.1$  and  $11.5 \pm 0.1$ , and stochasticity dominates at  $\text{pH } 6.5 \pm 0.1$ . Between pH values, both stochasticity and energetics contribute competitively to the fractal self-assembly of  $A\beta$ . This is also evident from the fact that,

instead of the expected morphologies solely governed by these kinetic models, mixed morphological characteristics were observed at different pH (Fig. 1). This indicates that  $m$  is expected to be in the range 0 to 0.05 for the  $A\beta$  self-assemblies. However, the exact determination of  $m$  would require more controlled experiments and is presently our ongoing subject of investigation.

#### IV. CONCLUDING REMARKS

The fractal self-assembly from a freshly prepared solution of  $A\beta$  under diffusion-limited conditions is experimentally demonstrated in two supporting media: DI water and PBS buffer. The confocal microscopy and FESEM with EDAX analysis were used to confirm that the fractal morphologies were from the protein and not from the salt present in the supporting media. The observations with  $A\beta$  solution at different pH helped us to understand the role of electrostatic interaction in the formation of fractal self-assemblies. The molecular docking experiments indicated the presence of nonexhaustive electrostatic and hydrophobic patches on the  $A\beta$  docked structures (oligomers) necessary for the propagation of the fractal self-assembly. The implications of the docking experiments were further checked by breaking matured fibrils of  $A\beta$  into smaller oligomers through sonication. The laser light experiments on the sonicated solutions and their drop casting indicated that oligomers with electrostatic and hydrophobic patches on their SASA interact to self-assemble into fractals. The  $R_g$  at different pH and the  $d_f$  of the fractal morphologies indicated the presence of a morphological phase transition from acidic pH (DLA-like fractals) to basic pH (BA-like dense and compact fractals) where a pH range close to pI acts

as a transition region. The morphological transition provides experimental evidence for the recently reported theoretical framework [19] for similar transitions.

The results of the present study provide a new dimension to the self-assembly of  $A\beta$  which may find potential applications in diagnosis, drug delivery, biosensing, and nanoparticle self-assemblies for targeted biomedical applications. Due to the high surface-to-volume ratio, the reported fractal self-assembly formed under appropriate conditions can efficiently enhance the drug delivery mechanism. Moreover, the structures of amyloids can be exploited for developing both nanoelectronic materials for biosensing and nanowires for optical applications [53]. Since for biosensing the surface of the structures are needed to be functionalized, their surface area is a decisive factor; thus, we believe that the fractal self-assembly of amyloid can be a promising candidate for sensing applications.

#### ACKNOWLEDGMENTS

This work is supported by the Department of Science and Technology, India, Grant No. CRG/2019/001684, project code KML. The authors thank and acknowledge Dr. Bogdan Barz, Forschungszentrum Jülich, Germany, for providing the modeled amyloid- $\beta$  monomer with  $\beta$ -sheet structures used for performing molecular docking experiments. The authors thank Somnath Maji, Department of Biotechnology, IIT Kharagpur, for his assistance in confocal microscopy imaging. A.S. and S.K. are thankful to the IIT Kharagpur central research facility for the equipment needed for carrying out the FESEM and HRTEM experimental measurements and MHRD for financial assistance.

- 
- [1] V. N. Uversky, C. J. Oldfield, and A. K. Dunker, *Annu. Rev. Biophys.* **37**, 215 (2008).
  - [2] I. W. Hamley, *Chem. Rev.* **112**, 5147 (2012).
  - [3] M. G. Iadanza, M. P. Jackson, E. W. Hewitt, N. A. Ranson, and S. E. Radford, *Nat. Rev. Mol. Cell Biol.* **19**, 755 (2018).
  - [4] G. Wei, Z. Su, N. P. Reynolds, P. Arosio, I. W. Hamley, E. Gazit, and R. Mezzenga, *Chem. Soc. Rev.* **46**, 4661 (2017).
  - [5] H. Yagi, T. Ban, K. Morigaki, H. Naiki, and Y. Goto, *Biochemistry* **46**, 15009 (2007).
  - [6] J.-P. Colletier, A. Laganowsky, M. Landau, M. Zhao, A. B. Soriaga, L. Goldschmidt, D. Flot, D. Cascio, M. R. Sawaya, and D. Eisenberg, *Proc. Natl. Acad. Sci. USA* **108**, 16938 (2011).
  - [7] N. E. Hernández, W. A. Hansen, D. Zhu, M. E. Shea, M. Khalid, V. Manichev, M. Putnins, M. Chen, A. G. Dodge, L. Yang *et al.*, *Nat. Chem.* **11**, 605 (2019).
  - [8] M. G. Herrera, L. A. Benedini, C. Lonez, P. L. Schilardi, T. Hellweg, J.-M. Ruyschaert, and V. I. Dodero, *Soft Matter* **11**, 8648 (2015).
  - [9] S. Khatun, A. Singh, S. Maji, T. K. Maiti, N. Pawar, and A. N. Gupta, *Soft Matter* **16**, 3143 (2020).
  - [10] T. S. Khire, J. Kundu, S. C. Kundu, and V. K. Yadavalli, *Soft Matter* **6**, 2066 (2010).
  - [11] A. Lomander, W. Hwang, and S. Zhang, *Nano Lett.* **5**, 1255 (2005).
  - [12] M. M. Murr and D. E. Morse, *Proc. Natl. Acad. Sci. USA* **102**, 11657 (2005).
  - [13] D. Pirici, C. Van Cauwenberghe, C. Van Broeckhoven, and S. Kumar-Singh, *Neurobiol. Aging* **32**, 1579 (2011).
  - [14] P. Ramanlal and L. M. Sander, *Phys. Rev. Lett.* **54**, 1828 (1985).
  - [15] T. A. Witten, Jr. and L. M. Sander, *Phys. Rev. Lett.* **47**, 1400 (1981).
  - [16] P. Meakin and F. Family, *Phys. Rev. A* **38**, 2110 (1988).
  - [17] K. Honda, H. Toyoki, and M. Matsushita, *J. Phys. Soc. Jpn.* **55**, 707 (1986).
  - [18] S. C. Ferreira, Jr, S. G. Alves, A. Faissal Brito, and J. G. Moreira, *Phys. Rev. E* **71**, 051402 (2005).
  - [19] J. Nicolás-Carlock, J. Carrillo-Estrada, and V. Dossetti, *Sci. Rep.* **7**, 1 (2017).
  - [20] P. Meakin and R. Jullien, *J. Chem. Phys.* **89**, 246 (1988).
  - [21] M. Rad-Malekshahi, L. Lempsink, M. Amidi, W. E. Hennink, and E. Mastrobattista, *Bioconjugate Chem.* **27**, 3 (2016).
  - [22] K. Rajagopal and J. P. Schneider, *Curr. Opin. Struct. Biol.* **14**, 480 (2004).
  - [23] W. Schärtl, *Light Scattering from Polymer Solutions and Nanoparticle Dispersions* (Springer Science & Business Media, Berlin, 2007).
  - [24] M. B. Huglin, *Light Scattering from Polymer Solutions* (Academic Press, New York, 1972).

- [25] ImageJ software, National Institutes of Health, Bethesda, MD, <http://rsbweb.nih.gov/ij/>.
- [26] T. Smith Jr, G. Lange, and W. B. Marks, *J. Neurosci. Methods* **69**, 123 (1996).
- [27] S. Jungblut, J.-O. Joswig, and A. Eychmüller, *Phys. Chem. Chem. Phys.* **21**, 5723 (2019).
- [28] Y. S. Kim, L. Liu, P. H. Axelsen, and R. M. Hochstrasser, *Proc. Natl. Acad. Sci. USA* **106**, 17751 (2009).
- [29] T. Wang, H. Jo, W. F. DeGrado, and M. Hong, *J. Am. Chem. Soc.* **139**, 6242 (2017).
- [30] A. N. Gupta and H. B. Bohidar, *Phys. Rev. E* **76**, 051912 (2007).
- [31] W. Zhao and H. Ai, *ChemPhysChem* **19**, 1103 (2018).
- [32] C. A. Paredes-Rosan, D. E. Valencia, H. L. Barazorda-Ccahuana, J. A. Aguilar-Pineda, and B. Gómez, *J. Mol. Model.* **26**, 1 (2020).
- [33] A. Aliyan, N. P. Cook, and A. A. Martí, *Chem. Rev.* **119**, 11819 (2019).
- [34] M. D'Amico, M. G. Di Carlo, M. Groenning, V. Militello, V. Vetri, and M. Leone, *J. Phys. Chem. Lett.* **3**, 1596 (2012).
- [35] See Supplemental Material at <http://link.aps.org/supplemental/10.1103/PhysRevE.104.064404> for results of the EDAX analysis, interface residues in the docked structures, molecular docking study performed with  $A\beta$  dimer, fractal self-assembly after 0 min and 2 min sonication, TEM image of matured fibrils of  $A\beta$  after 2 min sonication, fractal morphology of  $A\beta$  self-assembly at pH  $6.5 \pm 0.1$ , and FD calculation at pH  $11.5 \pm 0.1$ .
- [36] C. H. Tan, P. Ravi, S. Dai, and K. C. Tam, *Langmuir* **20**, 9901 (2004).
- [37] T. Yakhno, *J. Colloid Interface Sci.* **318**, 225 (2008).
- [38] B. Barz, A. K. Buell, and S. Nath, *Chem. Commun.* **57**, 947 (2021).
- [39] D. Kozakov, D. R. Hall, B. Xia, K. A. Porter, D. Padhorny, C. Yueh, D. Beglov, and S. Vajda, *Nat. Protoc.* **12**, 255 (2017).
- [40] M. Schmidt, A. Rohou, K. Lasker, J. K. Yadav, C. Schiene-Fischer, M. Fändrich, and N. Grigorieff, *Proc. Natl. Acad. Sci. USA* **112**, 11858 (2015).
- [41] R. Piazza, *Curr. Opin. Colloid Interface Sci.* **5**, 38 (2000).
- [42] D. N. Petsev and P. G. Vekilov, *Phys. Rev. Lett.* **84**, 1339 (2000).
- [43] D. Chandler, *Nature (London)* **437**, 640 (2005).
- [44] R. Piazza, *Curr. Opin. Colloid Interface Sci.* **8**, 515 (2004).
- [45] G. N. Patargias, S. A. Harris, and J. H. Harding, *J. Chem. Phys.* **132**, 235103 (2010).
- [46] P. Duarte-Neto, T. Stošić, B. Stošić, R. Lessa, and M. V. Milošević, *Phys. Rev. E* **90**, 012312 (2014).
- [47] V. A. Bogoyavlenskiy and N. A. Chernova, *Phys. Rev. E* **61**, 1629 (2000).
- [48] L. Niemeyer, L. Pietronero, and H. J. Wiesmann, *Phys. Rev. Lett.* **52**, 1033 (1984).
- [49] L. Pietronero, A. Erzan, and C. Evertsz, *Phys. Rev. Lett.* **61**, 861 (1988).
- [50] K. Kirshenbaum and V. Daggett, *Biochemistry* **34**, 7629 (1995).
- [51] A. Singh, S. Khatun, and A. N. Gupta, *Soft Matter* **16**, 7778 (2020).
- [52] J. Israelachvili and R. Pashley, *Nature (London)* **300**, 341 (1982).
- [53] A. Herland, D. Thomsson, O. Mirzov, I. G. Scheblykin, and O. Inganäs, *J. Mater. Chem.* **18**, 126 (2008).